Two-dimensional growth, anisotropic polaron transport, and magnetic phase segregation in epitaxial $Nd_{0.52}Sr_{0.48}MnO_3$ films

V. G. Prokhorov[a] and G. G. Kaminsky

Institute of Metal Physics, NASU, Kiev 03142, Ukraine

J. M. Kim, T. W. Eom, J. S. Park, and Y. P. Lee

q-Psi and Department of Physics, Hanyang University, Seoul 133-791, Korea

V. L. Svetchnikov

National Center for HREM, TU Delft, 2628AL, The Netherlands

G. G. Levtchenko, A. V. Paschenko, Yu. V. Medvedev, Yu. M. Nikolaenko, G. V. Bukin, and V. A. Khokhlov

Donetsk Institute of Physics and Technology, NASU, Donetsk 83114, Ukraine
(Submitted May 5, 2010)
Fiz. Nizk. Temp. **37**, 141–149 (February 2011)

$Nd_{0.52}Sr_{0.48}MnO_3$ films have been fabricated by dc magnetron sputtering on single-crystal $LaAlO_3$ (001) and $SrTiO_3$ (011) substrates with additional annealing to relax the lattice strain. Although the $Nd_{0.52}Sr_{0.48}MnO_3$ films were deposited simultaneously on different substrates at the same deposition rate, they differ in thickness by a factor of $\simeq\sqrt{2}$. The observed difference in thickness is explained by the two-dimensional (layer-by-layer) film growth, rather than by a difference in growth rate controlled by the crystalline orientation of the substrate. An analysis of optical and transport properties reveals that the observed anisotropy in the polaron motion is governed by a strong anisotropy in the trapping energy, rather than in polaron formation. It is shown that the deposited $Nd_{0.52}Sr_{0.48}MnO_3$ films exhibit magnetic behavior typical of two-phase magnetic systems and should be regarded as an assembly of interacting magnetic clusters.
 [doi:10.1063/1.3554368]

I. INTRODUCTION

The hole-doped manganites $L_{1-x}A_xMnO_3$, where L and A are a trivalent lanthanide ion and a divalent alkaline-earth ion, respectively, have attracted considerable attention because of their interesting fundamental properties, connected with colossal magnetoresistance (CMR), and their potential for applications.[1] However, practical development of these potential applications requires an understanding of some basic aspects of their structure-property relationships. The doped manganite perovskites exhibit a strong correlation between their lattice structure and magneto-transport properties, and this phenomenon becomes more important in thin films.[2–5] Consider thin $Nd_{0.52}Sr_{0.48}MnO_3$ films as an example. According to the phase diagram,[6] $Nd_{1-x}Sr_xMnO_3$ is a typical system whose ground state varies from a ferromagnetic (FM) metal to an A-type antiferromagnetic (AFM) metal when the Sr doping reaches 0.5. In addition, a charge-ordered (CO) phase with a so-called CE-type AFM structure is formed in a very narrow doping range near $x\approx 0.5$. At the same time, the ground state of this compound is drastically dependent on the degree of crystallinity, the lattice strain, the chemical homogeneity, and microstructure clustering, which are controlled by the fabrication technique. Thus the CO state can be stabilized by long-range lattice strain accumulated during film deposition.[7,8] CO CE-type AFM states can be suppressed by increasing the film thickness,[9] with a high hydrostatic pressure,[10,11] by decreasing the grain size in polycrystalline samples,[12,13] and by applying an electric field.[14] Therefore, the film crystallinity, the microstructure, and the epitaxial relationship to the substrate need to be fully controlled in order to obtain high-quality single- or multi-layer epitaxial films for specific applications.

Here we report some experiments on $Nd_{0.52}Sr_{0.48}MnO_3$ (NSMO) films deposited on single-crystal $LaAlO_3$ (001) and $SrTiO_3$ (011) substrates. The observed evidence of two-dimensional film growth and the significant differences in the physical properties of these films owing to crystal-lattice anisotropy, are discussed in detail.

II. EXPERIMENTAL TECHNIQUES

The films were prepared by dc magnetron sputtering at a substrate temperature of 650 °C.[15] To avoid the influence of lattice strain accumulated during deposition, the films were all annealed at 900 °C for 2 h in air. θ-2θ x-ray diffraction (XRD) patterns were obtained using a Rigaku diffractometer with Cu K_α radiation. The lattice parameters evaluated directly from the XRD data were plotted against $\cos 2\theta/\sin\theta$. The intercept of the extrapolated straight line to $\cos 2\theta/\sin\theta=0$ yielded a more precise value of the lattice parameter. High-resolution electron-microscopy (HREM) was carried out using a Philips CM300UT-FEG microscope with a field emission gun operated at 300 kV. The point resolution of the microscope was in the order of 0.12 nm. Cross-section specimens were prepared by the standard tech-

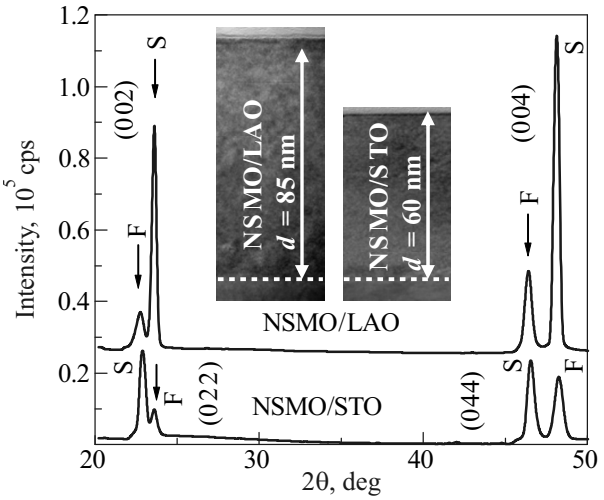

FIG. 1. XRD scans for NSMO/LAO and NSMO/STO films. F and S indicate the fundamental Bragg peaks for the film and the substrate, respectively. The insets are low-magnification cross-sectional HREM images taken at room temperature for the corresponding films. It can be seen that the films have different thicknesses.

niques using mechanical polishing followed by ion-beam milling at a grazing incidence. All the microstructure measurements were made at room temperature. Resistance measurements were made by the four-probe method over a temperature range of 4.2–300 K and in magnetic fields up to 5 T. The field-cooled (FC) and the zero-field-cooled (ZFC) magnetization curves were taken with a Quantum Design SQUID magnetometer with an in-plane magnetic field orientation. Magnetization curves for the bare substrates were extracted from the raw experimental curves. Optical-density (OD) spectra were obtained using a PGS-2 spectrograph from Carl Zeiss GmbH.

III. MICROSTRUCTURE AND TWO-DIMENSIONAL GROWTH OF FILMS

Figure 1 shows some θ-2θ XRD scans for the films, which were simultaneously deposited on $LaAlO_3$ (LAO) and $SrTiO_3$ (STO) substrates under the same conditions. Only the fundamental, high intensity Bragg peaks for the film (F) and the substrate (S) were observed, indicating that the deposition results in a highly oriented crystal structure. This is confirmed by analysis of the transmission contrast of the HREM images. At the same time, the cross-sectional low-magnification HREM images, shown in the insets in Fig. 1, show that the films have significantly different thicknesses (d=85 and 60 nm for the films deposited on LAO and STO, respectively), although the deposition rates for both were the same. Therefore, we may conclude that the film growth rates are different on the LAO (001) and the STO (011) substrates. This is to be expected, given that the growth rate for cubic crystals along the [100] orientation, as a rule, is significantly higher than that along [110]. It has been shown recently that the growth-rate ratio $s100/s110$ ranges from 1.2–1.8 for face-centered cubic structures.[16] In our case, assuming that the growth speed is d/t, where t is the deposition time, $s100/s110 \sim 1.42$, in good agreement with the theoretical prediction. However, other things also affect the thickness of films deposited on a single-crystal substrates.

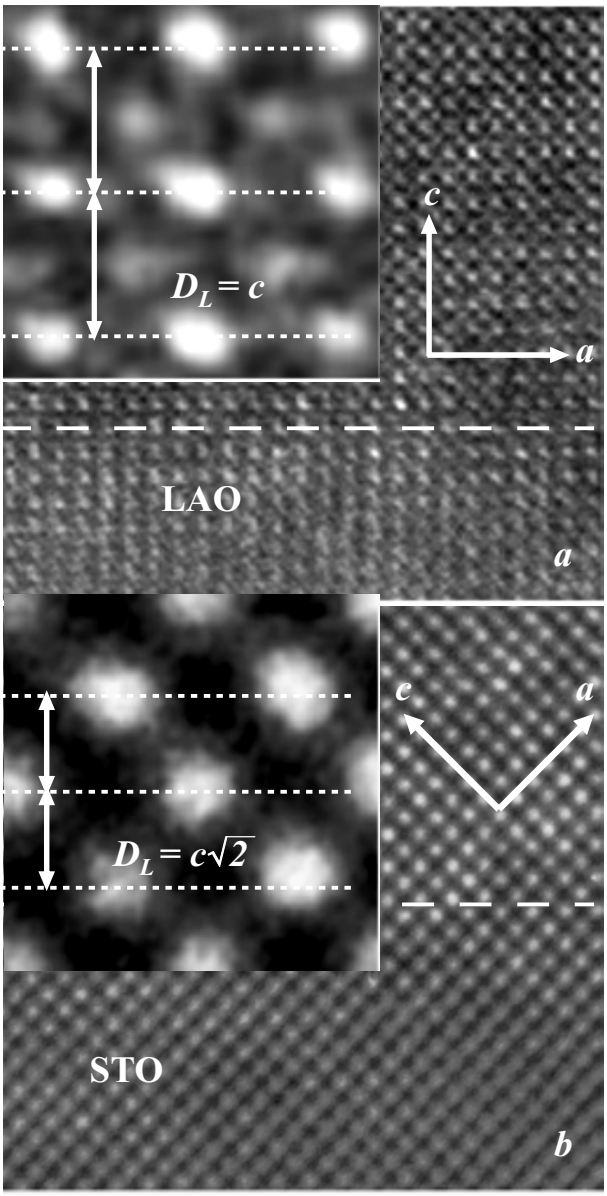

FIG. 2. High-magnification cross-sectional HREM images taken at room temperature for NSMO/LAO (*a*) and NSMO/STO (*b*) films. The dashed lines indicate the interface between film and substrate. *c* and *a* are the crystal lattice axes. The insets illustrate the atomic structure of the films in detail. *DL* denotes the atomic layer thickness.

Figure 2 shows cross-sectional high-magnification HREM images taken along the [010] axis for the films, deposited on LAO (*a*) and STO (*b*), including the film/substrate interfaces. Both films have an atomically clean and sharp interface without an amorphous intermediate layer or precipitates. The epitaxial relationships for film and substrate were found to be [001] NSMO$\|$[001] LAO and [011] NSMO$\|$[011] STO. The insets in Fig. 2 show that the distances between the rows of atoms (atomic layer thickness D_L) formed on the substrate surface during deposition are significantly different: $D_L=c$ and $c/\sqrt{2}$ for the NSMO/LAO and the NSMO/STO films, respectively, where c is the out-of-plane lattice parameter for cubic symmetry. This fact can help elucidate the growth mechanism.

Three kinds of growth mechanism are typical in thin films. These are the Volmer–Weber (island) mode, the

Frank–van der Merwe (layer) mode, and the intermediate Stranski–Krastanov (layer-plus-island) mode.[17] The well-defined atomic layered structure of the films (see Fig. 2) allows us to suggest that only the last two mechanisms are realized in our case, because both assume layer-by-layer film growth. Given that the layer-plus-island mode is preferable to the layer mode, because of adsorption-energy competition,[17] one can conclude that these films grow through the Stranski–Krastanov mechanism. Then the film thickness can be expressed as the product of the atomic-layer number (n_L) and layer thickness, $d=n_L D_L$. Even assuming that the number of layers is equal for both films, the thickness ratio for the NSMO/LAO and the NSMO/STO films differs with the difference in the layer thickness, i.e., $D_L^{\mathrm{LAO}}/D_L^{\mathrm{STO}} \simeq \sqrt{2}$. Thus, the observed difference in the thickness of the grown films follows from the special two-dimensional (layer-by-layer) film growth.

IV. EXPERIMENTAL RESULTS

Figure 3a shows OD spectra for the NSMO/LAO and the NSMO/STO films with $d=85$ and 60 nm, respectively, taken at room temperature. OD spectra for the bare substrates were extracted from the raw experimental curves. The first noticeable difference in optical properties between the NSMO/STO and NSMO/LAO films is in the transmission (T) value, which is higher by nearly an order of magnitude for the NSMO film deposited on the LAO (001) substrate. A similar peculiarity of the OD spectra for half-doped NSMO films has been observed previously at low temperatures, and explained by highly anisotropic orbital ordering.[7] On the other hand, the low-energy region in the optical spectra for manganites is identified as an incoherent background involving strong Jahn–Teller interactions with the polaron terms; this results in charge-transfer excitations from the oxygen $2p$-band states to bands involving the manganese e_g states near 3 eV.[18] Furthermore, crystal-field splitting governed by the Jahn–Teller effect would split the energies of the charge-transfer excitations and produce a fine structure in the central peak (indicated by arrows in Fig. 3a). The energy difference corresponds to charge-transfer excitation of ~76 and 73 meV, for NSMO/STO and NSMO/LAO, respectively. These values are very close to the polaron gap, which is typical for this compound at temperatures above the metal-insulator (MI) transition.[19]

Figure 3b shows the temperature dependence of the resistance, $R(T)$, without (open symbols) and with (solid symbols) an applied magnetic field of 5 T, for the same films. An analysis of the experimental $R(T)$ curves terms of the small-polaron motion model,[20] $R(T) \sim T \exp(E_A/k_B T)$, where E_A is an activation energy and k_B is the Boltzmann constant, yields $E_A=150$ and 110 meV, for NSMO/STO and NSMO/LAO, respectively.

Figure 4 shows the in-plane FC (solid symbols) and the ZFC (open symbols) temperature dependences of the magnetic moment, $M(T)$, for the NSMO/STO films with thickness $d=240$ (*a*), 120 (*b*) and 60 (*c*) nm at different applied magnetic fields. The ZFC and FC $M(T)$ curves were obtained for rising temperature after film cooling without and with an external magnetic field, respectively. All the films manifest an FM transition with decreasing temperature at a Curie temperature $T_C \sim 220$ K, which is very close to published data for this compound.[6,21] At the same time, the films manifest the well-defined ZFC/FC $M(T)$ splitting (even for high applied magnetic fields), which is typical for magnetic multiphase [cluster-glass or superparamagnetic (SPM)] systems. Coexistence of small-sized FM and AFM clusters at low temperatures has already been observed in similar compounds.[12,22,23] It has been shown, that the AFM clusters are caused by a crystal-lattice transition from an orthorhombic to a monoclinic phase at $T \leqslant T_N$ with the formation of a twin domain structure.[24] The Néel temperature, T_N, which was extracted from the reduced magnetic moment $M_{FC}/M_{ZFC}(T)$ curve (not shown),[25] also turned out to be the same for all the films, $T_N \sim 150$ K.

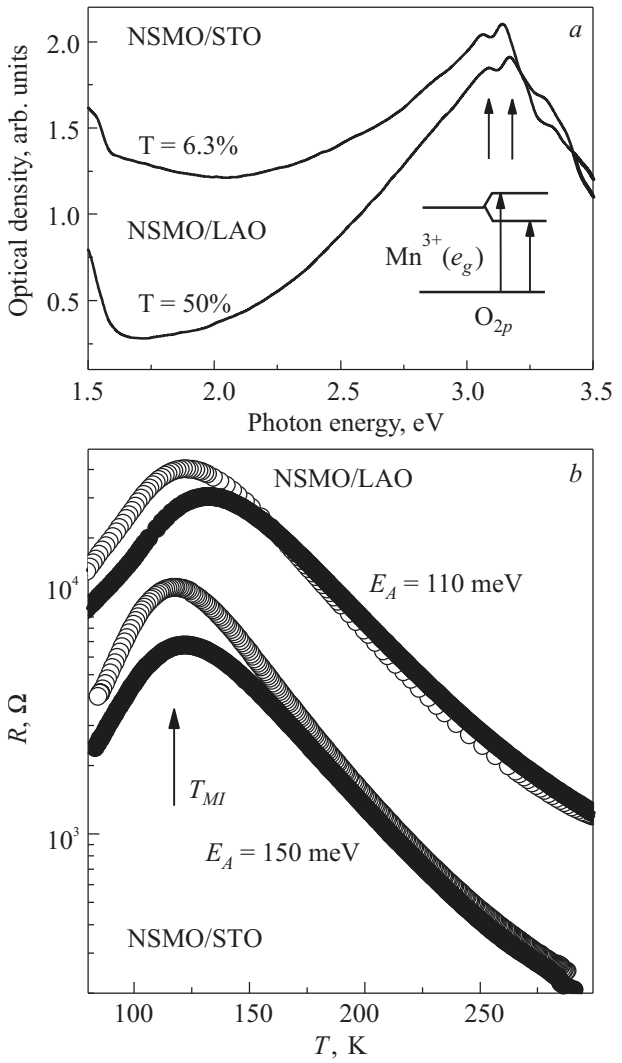

FIG. 3. (*a*) Optical-density spectra for NSMO/LAO and NSMO/STO films, taken at room temperature. T is the transmission. The arrows indicate the fine structure of a charge-transfer peak, governed by the e_g-level splitting. (*b*) Temperature dependence of the resistance for NSMO/LAO and NSMO/STO films, without (open symbols) and with (solid symbols) an applied magnetic field of 5 T. The arrow indicates the MI transition temperature. E_A is the activation energy derived from the small polaron model.

Figure 5 shows the analogous $M(T)$ curves for NSMO/LAO films with thicknesses $d=160$ (*a*), 110 (*b*) and 50 (*c*) nm at different applied magnetic fields. These films manifest a significant thickness dependence of the Curie temperature and a minor FC/ZFC $M(T)$ splitting (except for the thinnest

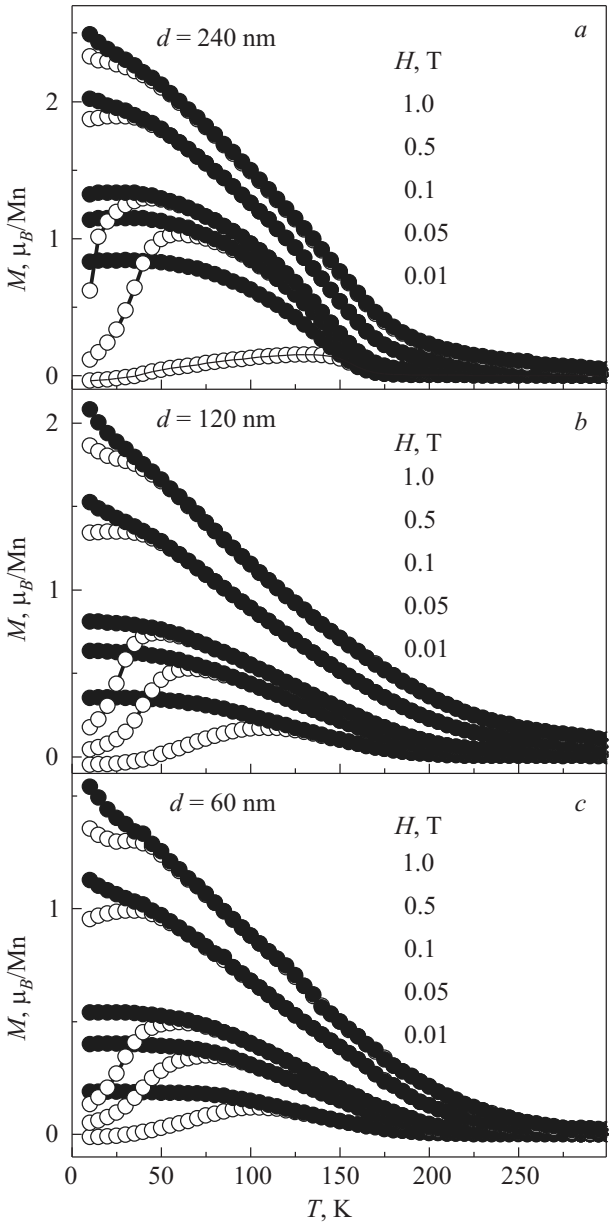

FIG. 4. Temperature dependence of the in-plane FC (solid symbols) and ZFC (open symbols) magnetic moments for the NSMO/STO films with thicknesses d=240 (*a*), 120 (*b*) and 60 (*c*) nm for different applied magnetic fields.

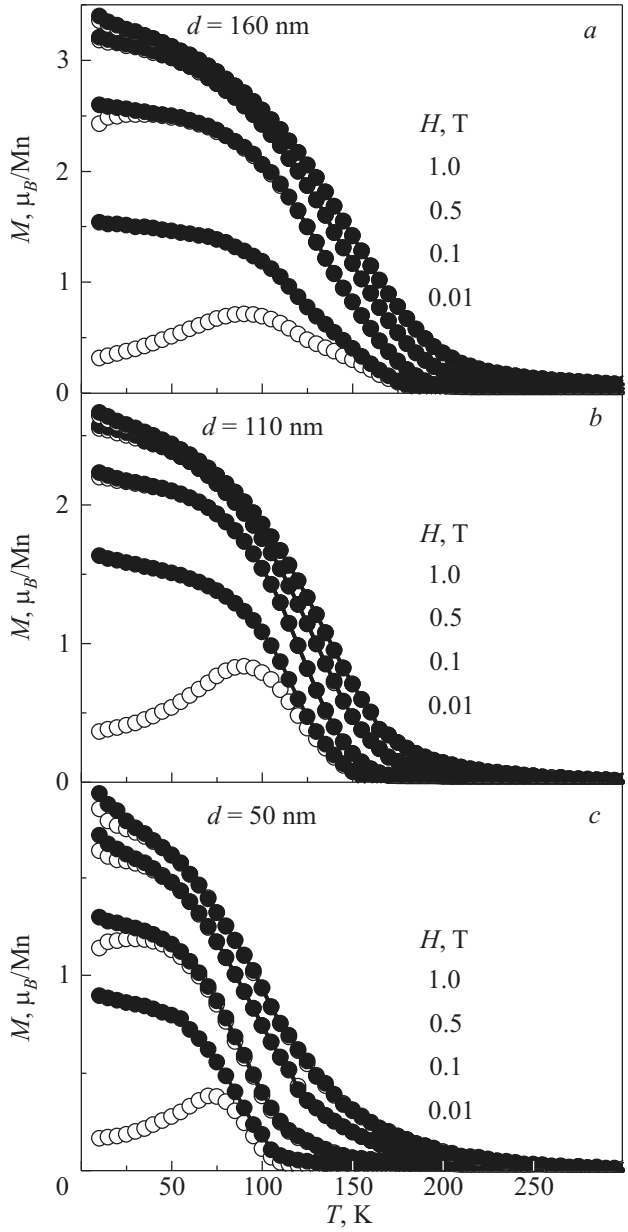

FIG. 5. Temperature dependence of the in-plane FC (solid symbols) and the ZFC (open symbols) magnetic moments for the NSMO/LAO films with thicknesses d=160 (*a*), 110 (*b*) and 50 (*c*) nm for different applied magnetic fields.

film), in contrast to the NSMO/STO films. At the same time, the Néel temperature is almost identical for these films, $T_N \sim 125$ K. Analysis of the $M(T)$ curves yields $T_C \sim 220$, 180 and 115 K for NSMO/LAO with d=160, 110 and 50 nm, respectively. Figure 6 illustrates the in-plane hysteresis loops, $M(H)$, at 10 K for NSMO/LAO (*a*) and NSMO/STO (*b*) films with different thicknesses. All these films were measured in the ZFC regime. It can be seen that the NSMO/LAO films have a much higher saturation magnetic moment M_s than the NSMO/STO films. Moreover, the $M(H)$ curves for the NSMO/STO films are unsaturated up to the highest magnetic field and manifest a linear increase with increasing magnetic field that implies the presence of an AFM phase. A similar unsaturated hysteresis loop is also observed in NSMO/LAO with $d \sim 50$ nm.

The major magnetic characteristics of the films are summarized in Table I.

V. DISCUSSION

We now examine the anisotropic origin of the polaron state observed in these films in more detail. In the adiabatic limit the activation energy for small-lattice-polaron (Holstein) motion involves two terms, $E_A = E_g/2 + W_H$, where E_g is the so-called trapping energy or the energy difference between the lattice distortion with and without a hole and W_H is the polaron formation energy.[20] The polaron formation energy in our case can be attributed to the energy splitting of the charge-transfer central peak (see inset in Fig. 3a), which is interpreted as a polaron gap, $W_H = \Delta_g$, and is almost the same for the NSMO/STO and NSMO/LAO films. At the same time, the difference between E_A and W_H, 74 and

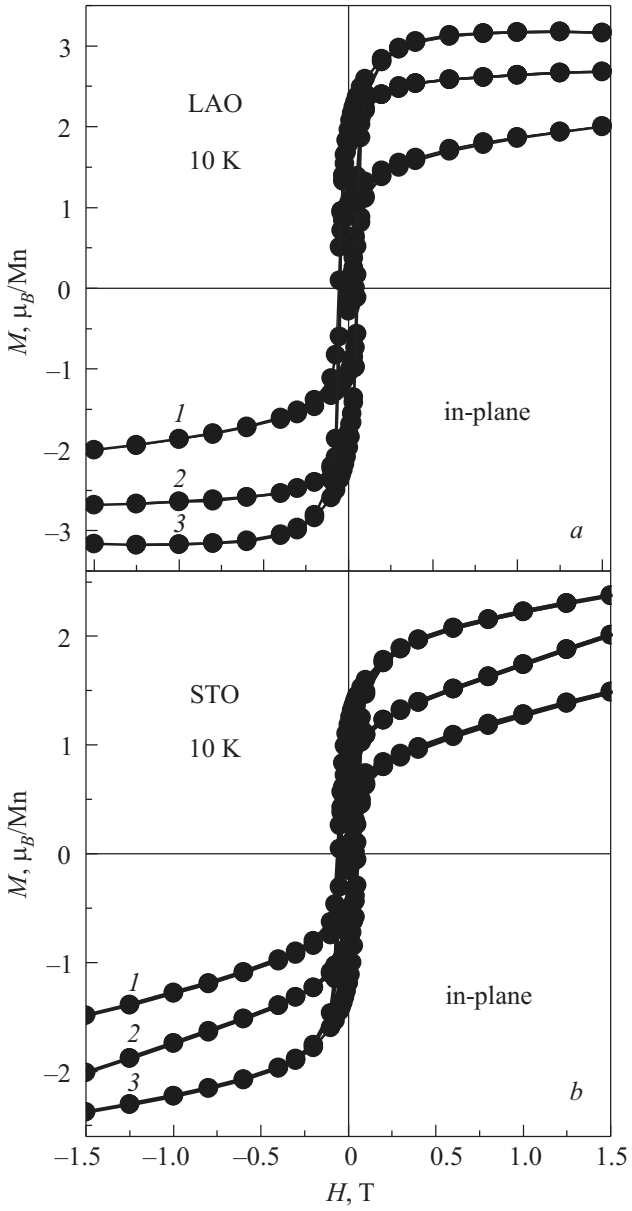

FIG. 6. Magnetic field dependences of the in-plane magnetic moment for (*a*) NSMO/LAO with d=50 (*1*), 110 (*2*) and 160 (*3*) nm, and (*b*) for NSMO/STO with d=60 (*1*), 120 (*2*) and 240 (*3*) nm, measured at 10 K. The curves are nominal fits.

37 meV for the NSMO/STO and NSMO/LAO films, respectively, is large for these films. Consequently, the observed anisotropy of the polaron motion is governed by a strong anisotropy of the trapping energy E_g, rather than of the polaron formation energy W_H.

Analysis of the $M(T)$ curves for these films (see Figs. 4 and 5) reveals that T_C is almost independent of the thickness for NSMO/STO but is very sensitive to the thickness for NSMO/LAO (see Table I). This phenomenon is mainly controlled by the lattice strain accumulated during epitaxial growth of the films, which greatly affects the formation of a spin-ordered state. Let us analyze our data using the Millis model.[26] For a weak lattice strain ε and cubic symmetry, T_C can be expressed as

$$T_C(\varepsilon) = T_{C0}\left(1 - \alpha\varepsilon_B - \frac{1}{2}\Delta\varepsilon_{JT}^2\right), \quad (1)$$

where $\alpha=(1/T_{C0})(dT_C/d\varepsilon_B)$, and $\Delta=(1/T_{C0})(d^2T_C/d\varepsilon_{JT}^2)$. The magnitudes of α and Δ represent the relative weights for the symmetry-conserving bulk strain ε_B and the symmetry-breaking Jahn–Teller strain ε_{JT}, respectively. According to the model, $\alpha\sim10$ for a reasonable electron-phonon coupling $(0.5\leqslant\lambda\leqslant1)$ in this compound, where λ is the electron-phonon-interaction constant, and $\Delta\sim5000$. The bulk strain $\varepsilon_B=(2\varepsilon_{100}+\varepsilon_{001})$ and the Jahn–Teller strain $\varepsilon_{JT}=\sqrt{2/3}(\varepsilon_{001}-\varepsilon_{100})$, where $\varepsilon_{100}=(a_{\text{bulk}}-a_{\text{film}})/a_{\text{bulk}}$ and $\varepsilon_{001}=(c_{\text{bulk}}-c_{\text{film}})/c_{\text{bulk}}$ are the in-plane and out-of-plane lattice strains. For example, let us consider the change in T_C predicted by the model for the NSMO/STO and NSMO/LAO films with the maximum and minimum thickness. Analysis of XRD and HREM data shows that the in-plane and out-of-plane lattice parameters for NSMO/STO correspond to $a\sim0.386$ and 0.387 nm and $c\sim0.3823$ and 0.381 nm for $d\sim240$ and 60 nm, respectively. Similar for NSMO/LAO: $a\sim0.384$ and 0.379 nm and $c\sim0.388$ and 0.394 nm for $d\sim160$ and 50 nm, respectively. The estimated values of ε_{100} and ε_{001} indicate that the NSMO/STO films have biaxial tensile in-plane and compressive out-of-plane lattice strains while the NSMO/LAO films are exposed to compressive in-plane and tensile out-of-plane strains. This is typical of manganite films deposited on the STO and LAO substrates.[27,28] Taking the Curie point and lattice parameters of thick films to be the same as the "bulk" material, we estimate the corresponding T_C values for NSMO/STO ($d\sim60$ nm) and NSMO/LAO ($d\sim50$ nm) to be 211 and 118 K, respectively, in excellent agreement with the experimental data (see Table I).

We can, therefore, conclude that the observed thickness dependence of the Curie temperature in the $Nd_{0.52}Sr_{0.48}MnO_3$ films, deposited on single-crystal $SrTiO_3$ (011) and $LaAlO_3$

TABLE I. Magnetic characteristics for the investigated films.

Samples	Thickness d, nm	Curie point T_C, K	Néel point T_N, K	Saturation magnetic moment M_s, μ_B/Mn	Remanence magnetic moment M_r, μ_B/Mn	Coercive field H_c, Oe
NSMO/STO	60	220	150	0.88	0.55	580
NSMO/STO	120	220	150	1.26	0.85	500
NSMO/STO	240	220	150	1.92	1.21	450
NSMO/LAO	50	115	125	1.71	1.11	600
NSMO/LAO	110	180	125	2.73	1.79	550
NSMO/LAO	160	220	125	3.45	2.03	500

(001) substrates is controlled by the sign and intensity of the accumulated lattice strains.

At the same time, according to the magnetic phase diagram $Nd_{0.52}Sr_{0.48}MnO_3$ undergoes an AFM transition (CE-type) at $T_N \leqslant 150$ K. The magnetic measurements (see Table I) indicate that the Néel temperature does not depend on thickness and is slightly lower for the NSMO/LAO films. As in the case of the Curie point, the observed slight difference in T_N between NSMO/STO and NSMO/LAO can be explained by the different lattice strain intensities in these films.

Figure 6 shows that the NSMO/LAO films have a higher saturation magnetic moment (M_s) and remanence (M_r) than the NSMO/STO films. Moreover, M_s and M_r decrease with decreasing thickness for both kinds of films. As a rule, the saturation magnetic moment per unit cell determines the volume of the FM phase in a sample. For NSMO/LAO with $d \sim 160$ nm $M_s \sim 3.45$ μ_B/Mn, while for NSMO/STO with $d \sim 240$ nm $M_s \sim 2$ μ_B/Mn. In addition, the $M(H)$ hysteresis loops for all the NSMO/STO films (as well as the thinnest NSMO/LAO) remain unsaturated up to highest applied magnetic field and manifest a linear increase in the magnetic moment with rising H, which is typical for the AFM phase. Therefore, the $Nd_{0.52}Sr_{0.48}MnO_3$ films can be treated as two-phase magnetic systems, the magnetic properties of which are controlled by the competition between ferromagnetic double-exchange and antiferromagnetic superexchange. On the other hand, the hole-doped perovskite manganites are strongly correlated systems and have a tendency toward phase separation, including the magnetic phase.[1] Therefore, the two magnetic phases are segregated into FM and AFM clusters and coexist for $T \leqslant T_N$.[22,29]

The main evidence for magnetic phase separation (or a magnetic clustering) is ZFC/FC $M(T)$ splitting, which was observed for all the NSMO/STO films and for the NSMO/LAO film with $d \sim 50$ nm over a wide range of applied magnetic fields (see Figs. 4 and 5). This phenomenon has been interpreted as a source of the glassy magnetic behavior and the phase segregated state treated as a cluster-glass or spin-glass-like phase.[30]

Figure 7a shows the magnetic field variations in the splitting point between the ZFC-FC $M(T)$ curves, $T^*(H)$, for NSMO/STO ($d \sim 60$, 120 and 240 nm) and NSMO/LAO ($d \sim 50$ nm). All the films have a strong and similar $T^*(H)$ dependence proportional to $\sim 1/H$.

According to the classical spin-glass model, the $T^*(H)$ curve is described by the Almeida-Thouless ZFC/FC $M(T)$ irreversibility line:[31]

$$T^*(H) = T^*(0)\left[1 - \left(\frac{3}{4}\frac{H^2}{J^2}\right)^{1/3}\right], \qquad (2)$$

where J is the exchange integral, which can be described by $J = 3k_B T_C/[2zS(S+1)]$, where T_C is the Curie temperature, $z = 6$ is the number of nearest neighbor atoms (because we assume a cubic unit cell), and $S = 1.74$ is the spin value (as an average of $S_1 = 2$ and $S_2 = 3/2$ corresponding to the Mn^{4+} and the Mn^{3+} ions, respectively). Figure 7a includes the Almeida–Thouless curve (ATL) obtained without any fitting parameters, using the experimental values for the Curie point (220 K) and the saturation magnetic moment for the complete FM state (~ 3.45 μ_B/Mn). The theoretical curve has a weaker $T^*(H)$ dependence than the experimental data. An alternative cluster-glass (or droplet) model,[32] which includes a field dependence for the magnetic correlation length, predicts a strong rise of T^* with increasing magnetic field, in contrast with our results.[30]

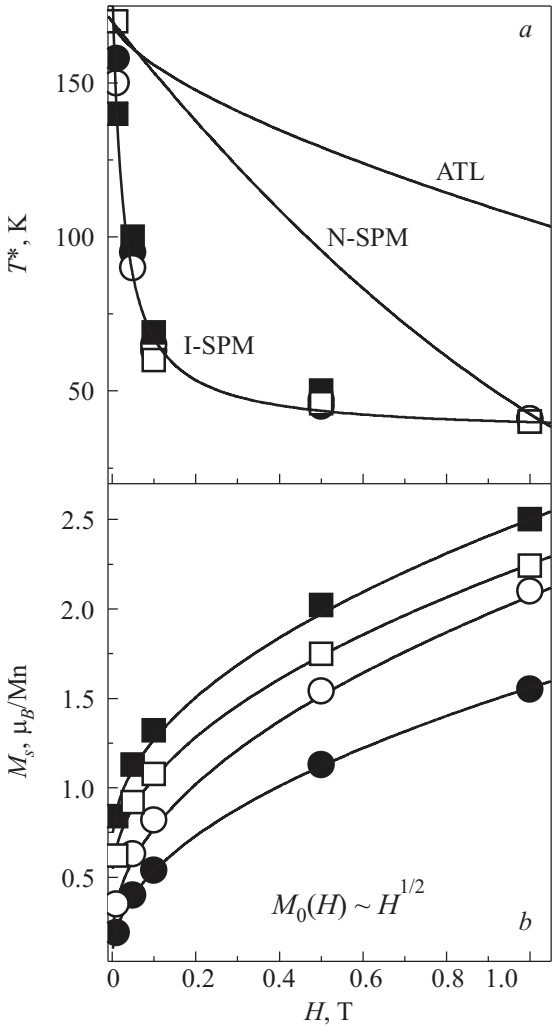

FIG. 7. (*a*) Magnetic field dependences of the splitting point between the ZFC-FC $M(T)$ curves, $T^*(H)$, for NSMO/STO [$d \sim 60$ (solid squares), 120 (open circles) and 240 nm (solid circles)] and NSMO/LAO [$d \sim 50$ nm (open squares)] films. The solid curves are theoretical values predicted by the spin-glass (ATL), noninteracting superparamagnet (N-SPM), and interacting superparamagnet (I-SPM) models. (*b*) Magnetic field dependences of the saturation magnetic moment derived from the FC $M(T)$ experimental curves for the same films. The solid curves are the fit curves described in text.

On the other hand, the magnetic phase-separated state can be regarded as an ensemble of superparamagnetic (SPM) particles. In this case T^* is equivalent to a blocking temperature (T_B), given by $k_B T_B \sim KV_{SPM}$,[33,34] above which the magnetic moments of the SPM particles move freely owing to thermal fluctuations while they shift into the blocked state at $T \leqslant T_B$. Here KV_{SPM} is the energy barrier between two directions of the magnetic moment in a single SPM particle, parallel and opposite to the applied magnetic field, and K is the magnetic anisotropy constant. For noninteracting SPM particles $T_B(H)$ is given by[35,36]

$$T_B(H) = T_B(0)\left(1 - \frac{H}{H_0}\right)^2, \quad (3)$$

where $T_B(0)$ is the blocking temperature without a magnetic field and $H_0 = 2K/\mu_0 M_s$. The theoretical curve, denoted as N-SPM, was calculated using experimental data, $K \sim 8.4 \cdot 10^4$ J·m^{-3} (for an $Nd_{0.5}Sr_{0.5}MnO_3$ film)[3,4] and $M_s \sim 3.45\ \mu_B$/Mn. However, as in the spin-glass-like model, a significant disagreement between the experimental and theoretical $T_B(H)$ dependences is also observed.

Lately the model of an interacting superparamagnetic (I-SPM) phase has been used to analyze SPM materials, including the strong dipolar interaction between SPM clusters.[4,37–40] Apart from the direct numerical simulations, the dipolar interaction is introduced by properly modifying the argument of the Langevin function for the noninteracting SPM particles: $\mu_{\text{eff}}H/k_BT \rightarrow \mu H/k_B\ (T+T_D)$, where $2T_D = \alpha M_0/k_BN$ is the so-called "dipolar temperature," α is a constant on the order of unity, N is the number of Mn ions per unit volume, and M_0 is the magnetic moment at $T=0$ K, taken from the $M(T)$ experimental curves for different applied magnetic fields. Since $\mu_{\text{eff}} \sim V_{\text{SPM}} \sim T_B$ and $N=1$ in our case, we can write

$$T_B(H) = T_B(0)\frac{1}{[1 + \alpha M_0^2/k_BT]}. \quad (4)$$

Figure 7b shows that the magnetic field dependences of M_0 for the NSMO/STO films can be excellently fitted by the universal function $M_0(H)/AH^{1/2}$, where A is varied from 1.9 to 1.5 $\mu_B \cdot \text{T}^{-1/2}$ as the thickness decreases. Therefore, Eq. (4) can be modified to $T_B(H) = T_B(0)/(1+\beta H)$, where $\beta = \alpha A^2/k_BT$. Figure 7a shows that the theoretical curve with the fit parameters $T_B(0) = 140$ K and $\beta = 35$ T^{-1}, indicated by I-SPM, is in excellent agreement with the experimental curve.

The NSMO/STO films (and thinnest NSMO/LAO) can, therefore, be treated as interacting SPM systems rather than classical spin glasses or the Langevin-like SPMs. At the same time ZFC/FC $M(T)$ splitting can hardly be seen in the thick NSMO/LAO films (see Figs. 5a and 5b). This is explained by the large volume of the FM phase in the films, which is confirmed by the large values of M_s per unit cell (see Table I). In this case the concentration of the FM phase exceeds a percolating threshold value for an infinite FM cluster and the SPM-like effects cannot be observed.

VI. CONCLUSIONS

We have measured microstructure, optical, transport, and magnetic properties of $Nd_{0.52}Sr_{0.48}MnO_3$ films prepared by dc magnetron sputtering on single-crystal $LaAlO_3$ (001) and $SrTiO_3$ (011) substrates with additional annealing to relax the lattice strain. Our major results can be summarized as follows:

(1) The θ-2θ XRD scans and the HREM images reveal that the NSMO/LAO and NSMO/STO films have a perfect microstructure and a highly oriented crystal structure with [001] NSMO‖[001] LAO and [011] NSMO‖[011] STO epitaxial relationships, respectively. On the other hand, even though the $Nd_{0.52}Sr_{0.48}MnO_3$ films were deposited simultaneously on different substrates at the same deposition rate, they differ in thickness by a factor of $\simeq\sqrt{2}$. The observed difference is explained by the two-dimensional (layer-by-layer) film growth rather than by a difference in the growth rate, controlled by the crystal orientation of substrate.

(2) The optical-density spectra show that the transmission is higher by nearly an order of magnitude for the NSMO/LAO film than for the NSMO/STO film. This is explained by an anisotropic origin of the Jahn–Teller interactions which leads to anisotropy of the polaron state in this compound. Moreover, the observed slight splitting of the central peak, corresponding to charge-transfer excitations from oxygen $2p$-band states to bands involving manganese e_g states near 3 eV, indicates that polaron gaps of ~76 and 73 meV, for NSMO/STO and NSMO/LAO, respectively, develop in the films.

(3) The $R(T)$ curves measured for temperatures above the MI transition indicate a thermally activated behavior and can be described in terms of a small-polaron motion model with activation energies $E_A = 150$ and 110 meV for NSMO/STO and NSMO/LAO, respectively. Since the polaron gap derived from the OD spectra is almost the same for both kinds of films, one can conclude that the observed anisotropy in the polaron motion is governed by a strong anisotropy of the trapping energy rather than of the polaron formation energy.

(4) It was found that the observed dependence of the Curie temperature on thickness for the $Nd_{0.52}Sr_{0.48}MnO_3$ films deposited on $SrTiO_3$ (011) and $LaAlO_3$ (001) substrates is controlled by the sign and intensity of the accumulated lattice strain.

(5) Analysis of the magnetic properties shows that the $Nd_{0.52}Sr_{0.48}MnO_3$ films can be treated as two-phase magnetic systems, the magnetic properties of which are controlled by the competition between ferromagnetic double-exchange and antiferromagnetic superexchange. Magnetic phase segregation in FM and AFM clusters, which coexist for $T \leqslant T_N$, is confirmed by splitting of the measured ZFC/FC $M(T)$ curves for different applied magnetic fields. In contrast to the bulk material[22] and half-doped thin film,[7] in our case the AFM phase arises from a precursor paramagnetic state, rather than from the formed FM state. At the same time, the SPM-like clustering state occurs when the concentration of the FM phase does not exceed a percolating threshold value. The observed tendency of the (011)-oriented films to undergo phase separation is explained by a smaller volume of the FM phase than in the (001)-oriented films.

(6) A comprehensive analysis of the spin-glass-like and SPM approaches reveals that the deposited $Nd_{0.52}Sr_{0.48}MnO_3$ films should be regarded as an assembly of interacting magnetic clusters, quite similar to SPM particles with a dipolar interaction, at least in terms of their magnetic behavior.

This work was supported by the NRF/MEST through the Quantum Photonic Science Research Center, Korea.

V. Svetchnikov is grateful to the financial support of Netherlands Institute for Metal Research.

[a)]Email: pvg@imp.kiev.ua

[1]For a review, see Colossal Magnetoresistance, Charge Ordering and Related Properties of Manganese Oxides, C. N. R. Rao and B. Raveau (eds.), World Scientific, Singapore (1998); Colossal Magnetoresistance Oxides, Y. Tokura (ed.), Gordon and Breach, London (1999); E. Dagotto, T. Hotta, and A. Moreo, Phys. Rep. **344**, 1 (2001).
[2]F. Tsui, M. C. Smoak, T. K. Nath, and C. B. Eom, Appl. Phys. Lett. **76**, 2421 (2000).
[3]V. G. Prokhorov, G. G. Kaminsky, V. A. Komashko, Y. P. Lee, S. Y. Park, Y. H. Hyun, J. B. Kim, J. S. Park, V. L. Svetchnikov, V. P. Pashchenko, and V. A. Khokhlov, Fiz. Nizk. Temp. **33**, 889 (2007) [Low Temp. Phys. **33**, 678 (2007)].
[4]V. G. Prokhorov, Y. H. Hyun, J. S. Park, J. B. Kim, G. H. Kim, Y. S. Lee, Y. P. Lee, and V. L. Svetchnikov, J. Appl. Phys. **104**, 103901 (2008).
[5]Y. H. Hyun, S. Y. Park, Y. P. Lee, V. G. Prokhorov, and V. L. Svetchnikov, Appl. Phys. Lett. **91**, 262505 (2007).
[6]R. Kajimoto, H. Yoshizawa, H. Kawano, H. Kuwahara, Y. Tokura, K. Ohoyama, and M. Ohashi, Phys. Rev. B **60**, 6506 (1999).
[7]Y. Ogimoto, M. Nakamura, N. Takubo, H. Tamaru, M. Izumi, and K. Miyano, Phys. Rev. B **71**, 060403 (2005).
[8]M. J. Calderyn, A. J. Millis, and K. H. Ahn, Phys. Rev. B **68**, 100401 (2003).
[9]Q. Qian, T. A. Tyson, C.-C. Kao, W. Prellier, J. Bai, A. Biswas, and R. L. Greene, Phys. Rev. B **63**, 224424 (2001).
[10]C. Cui, T. A. Tyson, Z. Chen, and Z. Zhong, Phys. Rev. B **68**, 214417 (2003).
[11]R. C. Yu, J. Tang, L. D. Yao, A. Matsushita, Y. Yu, F. Y. Li, and C. Q. Jin, J. Appl. Phys. **97**, 083910 (2005).
[12]P. Levy, F. Parisi, G. Polla, D. Vega, G. Leyva, H. Lanza, R. S. Freitas, and L. Ghivelder, Phys. Rev. B **62**, 6437 (2000).
[13]S. Dong, F. Gao, Z. Q. Wang, J. M. Liu, and Z. F. Ren, Appl. Phys. Lett. **90**, 082508 (2007).
[14]V. Ponnambalam, S. Parashar, A. R. Raju, and C. N. R. Rao, Appl. Phys. Lett. **74**, 206 (1999).
[15]V. N. Varyukhin, Yu. V. Medvedev, Yu. M. Nikolaenko, A. B. Mukhin, B. V. Belyaev, V. A. Gritskikh, I. V. Zhikharev, S. V. Kara-Murza, N. V. Korchikova, and A. A. Tikhii, Tech. Phys. Lett. **35**, 937 (2009).
[16]G. Tegze, L. Gránásy, G. I. Tyth, F. Podmaniczky, A. Jaatinen, T. Ala-Nissila, and T. Pusztai, Phys. Rev. Lett. **103**, 035702 (2009).
[17]J. A. Venables, G. D. T. Spiller, and M. Hanbücken, Rep. Prog. Phys. **47**, 399 (1984).
[18]A. Rusydi, R. Rauer, G. Neuber, M. Bastjan, I. Mahns, S. Müller, P. Saichu, B. Schulz, S. G. Singer, A. I. Lichtenstein, D. Qi, X. Gao, X. Yu, A. T. S. Wee, G. Stryganyuk, K. Dörr, G. A. Sawatzky, S. L. Cooper, and M. Rübhausen, Phys. Rev. B **78**, 125110 (2008).
[19]M. Quijada, J. Černe, J. R. Simpson, H. D. Drew, K. H. Ahn, A. J. Millis, R. Shreekala, R. Ramesh, M. Rajeswari, and T. Venkatesan, Phys. Rev. B **58**, 16093 (1998).
[20]E. Iguchi, K. Ueda, and W. Jung, Phys. Rev. B **54**, 17431 (1996).
[21]P. Wagner, I. Gordon, L. Trappeniers, J. Vanacken, F. Herlach, V. V. Moshchalkov, and Y. Bruynseraede, Phys. Rev. Lett. **81**, 3980 (1998).
[22]Z. Q. Li, H. Liu, Y. H. Cheng, W. B. Mi, A. Yu, H. L. Bai, and E. I. Jiang, Physica B **353**, 324 (2004).
[23]P. W. Kolb, D. B. Romero, H. D. Drew, Y. Moritomo, A. B. Souchkov, and S. B. Ogale, Phys. Rev. B **70**, 224415 (2004).
[24]V. Eremenko, S. Gnatchenko, N. Makedonska, Yu. Shabakayeva, M. Shvedun, V. Sirenko, J. Fink-Finowicki, K. V. Kamenev, G. Balakrishnan, and D. McK Paul, Fiz. Nizk. Temp. **27**, 1258 (2001) [Low Temp. Phys. **27**, 930 (2001)].
[25]Y. H. Hyun, J. S. Park, T. W. Eom, G. H. Kim, Y. S. Lee, Y. P. Lee, V. G. Prokhorov, and V. L. Svetchnikov, Appl. Phys. Lett. **93**, 042515 (2008).
[26]A. J. Millis, T. Darling, and A. Migliori, J. Appl. Phys. **83**, 1588 (1998).
[27]V. G. Prokhorov, V. A. Komashko, G. G. Kaminsky, K. K. Yu, S. J. Jun, S. Y. Park, J. S. Park, Y. P. Lee, and V. L. Svetchnikov, Fiz. Nizk. Temp. **33**, 78 (2007) [Low Temp. Phys. **33**, 58 (2007)].
[28]Y. P. Lee, S. Y. Park, Y. H. Hyun, J. B. Kim, V. G. Prokhorov, V. A. Komashko, and V. L. Svetchnikov, Phys. Rev. B **73**, 224413 (2006).
[29]I. O. Shklyarevskiy, M. Yu. Shvedun, S. L. Gnatchenko, P. J. M. van Bentum, P. C. Cristianen, J. C. Maan, and K. V. Kamenev, Fiz. Nizk. Temp. **27**, 1250 (2001) [Low Temp. Phys. **27**, 923 (2001)].
[30]F. Rivadulla, M. A. Lypez-Quitela, and J. Rivas, Phys. Rev. Lett. **93**, 167206 (2004).
[31]J. R. L. de Almaida and D. J. Thouless, J. Phys. A **11**, 983 (1978).
[32]D. S. Fisher and D. A. Huse, Phys. Rev. B **38**, 373 (1988).
[33]L. Néel, C. R. Acad. Sci. URSS **228**, 664 (1949).
[34]W. F. Brown, Phys. Rev. **130**, 1677 (1963).
[35]R. W. Chantrell and P. Wohlfarth, Phys. Status Solidi A **91**, 619 (1985).
[36]R. Skomski, J. Phys.: Condens. Matter **15**, 841 (2003).
[37]J. Du, B. Zhang, R. K. Zheng, and X. X. Zhang, Phys. Rev. B **75**, 014415 (2007).
[38]P. Allia, M. Coisson, P. Tiberto, F. Vinai, M. Knobel, M. A. Novak, and W. C. Nunes, Phys. Rev. B **64**, 144420 (2001).
[39]O. Margeat, M. Tran, M. Spasova, and M. Farle, Phys. Rev. B **75**, 134410 (2007).
[40]P. Allia, F. Celegato, M. Coisson, A. Da Re, F. Ronconi, F. Spizzo, P. Tiberto, and F. Vinai, J. Magn. Magn. Mater. **290–291**, 580 (2005).

This article was published in English in the original Russian journal. Reproduced here with stylistic changes by AIP.